Membrane perturbation, altered morphology and killing of Staphylococcus epidermidis upon contact with a cytocompatible peptide-based antibacterial

Journal Pre-proof

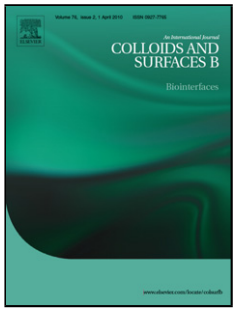

Membrane perturbation, altered morphology and killing of *Staphylococcus epidermidis* upon contact with a cytocompatible peptide-based antibacterial surface

Gerard Boix-Lemonche (Conceptualization) (Methodology) (Validation) (Data curation) (Formal analysis) (Investigation) (Visualization) (Writing - original draft) (Writing - review and editing), Jordi Guillem-Marti (Conceptualization) (Investigation) (Validation) (Data curation) (Writing - review and editing), Maria Lekka (Resources) (Investigation) (Writing - review and editing), Francesca D'Este (Resources) (Investigation) (Formal analysis) (Writing - review and editing), Filomena Guida<ce:contributor-role>Resources) (Investigation), José María Manero (Supervision) (Funding acquisition) (Writing - review and editing), Barbara Skerlavaj (Supervision) (Project administration) (Funding acquisition) (Writing - review and editing)

PII: S0927-7765(21)00189-2

DOI: https://doi.org/10.1016/j.colsurfb.2021.111745

Reference: COLSUB 111745

To appear in: *Colloids and Surfaces B: Biointerfaces*

Received Date: 9 December 2020

Revised Date: 8 March 2021

Accepted Date: 1 April 2021

Please cite this article as: Boix-Lemonche G, Guillem-Marti J, Lekka M, D'Este F, Guida F, Manero JM, Skerlavaj B, Membrane perturbation, altered morphology and killing of *Staphylococcus epidermidis* upon contact with a cytocompatible peptide-based antibacterial surface, *Colloids and Surfaces B: Biointerfaces* (2021), doi: https://doi.org/10.1016/j.colsurfb.2021.111745

Membrane perturbation, altered morphology and killing of *Staphylococcus epidermidis* upon contact with a cytocompatible peptide-based antibacterial surface

Gerard Boix-Lemonche[a,1]; Jordi Guillem-Marti[b,c]; Maria Lekka[d,e]; Francesca D'Este[a]; Filomena Guida[f]; José María Manero[b,c]; Barbara Skerlavaj[a,*]

[a]Department of Medicine (DAME); University of Udine; piazzale Kolbe, 4, 33100 Udine; Italy.

[b]Biomaterials, Biomechanics and Tissue Engineering Group, Department of Materials Science and Engineering; Universitat Politècnica de Catalunya (UPC); Av. Eduard Maristany 14, 08930 Barcelona; Spain.

[c]Barcelona Research Center in Multiscale Science and Engineering-UPC; Av. Eduard Maristany 14, 08930, Barcelona; Spain.

[d]University of Udine, Polytechnic Department of Engineering and Architecture, Via delle Scienze 206, 33100, Udine, Italy.

[e]CIDETEC, Basque Research and Technology Alliance (BRTA); Po. Miramón 196, 20014 Donostia-San Sebastián, Spain.

[f]University of Trieste, Department of Life Sciences, Via Giorgieri 5, 34127, Trieste, Italy.

[1]Present address: Center for Eye Research, Department of Ophthalmology, Institute of Clinical Medicine, Faculty of Medicine, University of Oslo.

*Corresponding author at:

Department of Medicine (DAME); University of Udine; piazzale Kolbe, 4, 33100 Udine; Italy;

e-mail: barbara.skerlavaj@uniud.it

Author's e-mail addresses:

Boix-Lemonche, Gerard: gerardboixlemonche@gmail.com;

Guillem-Marti, Jordi: jordi.guillem.marti@upc.edu;

Lekka, Maria: maria.lekka@uniud.it;

D'Este, Francesca: francesca.deste@uniud.it;

Guida, Filomena: milenaguida@gmail.com;

Manero, José María: jose.maria.manero@upc.edu;

Statistical Summary

Number of words	6001
Number of Figures	8

Graphical abstract

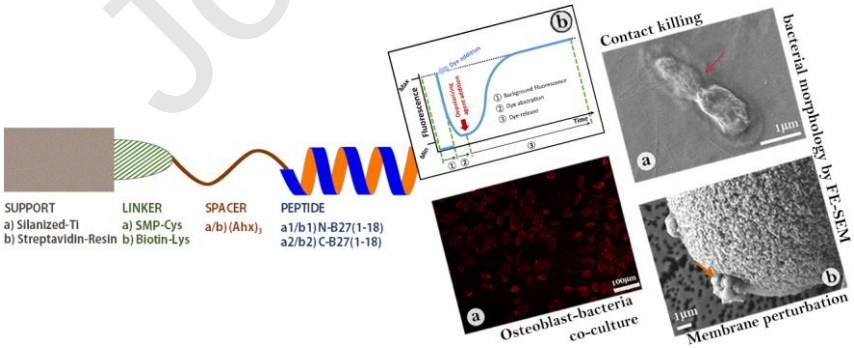

Highlights

- A membrane-active bactericidal peptide was linked to titanium and to a model resin
- SEM images of dead bacteria support contact-killing by the peptide-modified surfaces
- A fluorescent assay reveals faster membrane perturbation by the C- resin-bound analog
- N- and C-anchored analogs improved osteoblast adhesion to titanium to the same extent
- Osteoblast adhesion was equally improved also upon co-culture with bacteria

Abstract

One possibility to prevent prosthetic infections is to produce biomaterials resistant to bacterial colonization by anchoring membrane active antimicrobial peptides (AMPs) onto the implant surface. In this perspective, a deeper understanding of the mode of action of the immobilized peptides should improve the development of AMP-inspired infection-resistant biomaterials. The aim of the present study was to characterize the bactericidal mechanism against *Staphylococcus epidermidis* of the AMP BMAP27(1-18), immobilized on titanium disks and on a model resin support, by applying viability counts, Field Emission Scanning Electron Microscopy (FE-SEM), and a fluorescence microplate assay with a membrane potential-sensitive dye. The cytocompatibility to osteoblast-like MG-63 cells was investigated in monoculture and in co-culture with bacteria. The impact of peptide orientation was explored by using N- and C- anchored analogues. On titanium, the ~50% drop in bacteria viability and dramatically affected morphology indicate a contact-killing action exerted by the N- and C-immobilized peptides to the same extent. As further shown by the fluorescence assay with the resin-anchored peptides, the bactericidal effect was mediated by rapid membrane perturbation, similar to free peptides. However, at peptide MBC resin equivalents the C-oriented analogue proved more effective with more than 99% killing and maximum fluorescence increase, compared to half-maximum fluorescence with more than 90% killing produced by the N-orientation. Confocal microscopy analyses revealed 4-5 times better MG-63 cell adhesion on peptide-functionalized titanium both in monoculture and in co-culture with bacteria, regardless of peptide orientation, thus stimulating further studies on the effects of the immobilized BMAP27(1-18) on osteoblast cells.

Keywords: Bactericidal biomaterial, Antimicrobial peptide-functionalized titanium, Fluorescence microplate assay, Osteoblast-bacteria co-culture, bacterial morphology by FE-SEM

1. Introduction

Periprosthetic joint infection (PJI) is a devastating complication in prosthetic surgery that can lead to prosthesis loosening and failure[1]. It occurs in 1-2% of primary and in 4% of revision arthroplasties and requires complex treatment schemes[2]. Coagulase-negative *Staphylococci* (CoNS) have been isolated in about 30-50% of the cases, followed by *Staphylococcus aureus* in 10-45% of them[3,4]. *S. aureus* is considered a high-virulent microorganism and is principally responsible of early acute infection, while CoNS are considered low-virulent pathogens and are most frequently isolated from delayed chronic infections[2]. Among CoNS, *S. epidermidis* is the leading causative organism of foreign body related infections, including PJIs, due to its capacity to adhere to implanted devices and form biofilm[3,4]. Biofilm formation on the surface of implanted prostheses makes the treatment of PJIs challenging due to the limited number of antibiotics effective against biofilm. Based on clinical experience, complex treatment algorithms have been established[2].

One alternative strategy, which is still at a preclinical level, aims to prevent PJIs by making biomaterials intrinsically resistant to bacterial colonization. For this purpose, the material surface should be endowed with long-lasting antimicrobial properties. Several different approaches have been pursued, including covalent grafting of antimicrobial agents onto the biomaterial surface[5–7]. In this perspective, the antimicrobial peptides (AMPs) [8,9] are considered as good candidates due to rapid bactericidal activity[10,11] and low propensity for selection of resistant mutants[12]. The most suitable AMPs for covalent immobilization are those targeting the bacterial membrane as they are supposed to retain activity in the immobilized condition, opposite to drugs which activity relies on internal targets. Various AMPs have been anchored to titanium (and other medical materials) with promising results in terms of antimicrobial efficacy and biocompatibility[13,14]. For further improvement of peptide-functionalized biomaterials, we should be able to better design peptide derivatives and to apply the most appropriate coupling chemistry. To this aim, we would need a

deeper understanding of the mode of action of the candidate peptides in the immobilized state. In the last decade, a lively debate has arisen concerning immobilized AMP's activity and mode of action[15–18] as, in general, a reduced activity of the immobilized molecules, respect to their soluble counterparts, was observed. For some membrane active AMPs it was established that a flexible spacer of a minimum length was necessary to allow sufficient peptide mobility[7,15,19,20]. Moreover, in several cases peptide orientation also proved important, though opposite results were found when using different peptide molecules[16,17,21–23]. Hence, we are not able to extrapolate a general rule as each peptide sequence shows its own specificity. In addition, the issue is not easy to address from a technical point of view, due to the lack of specific techniques for mode of action studies with surface immobilized peptides. Researchers have to find novel approaches or to adapt known techniques to peptides, immobilized on a suitable model surface.

The antimicrobial peptide BMAP27(1-18) has been shown to maintain bactericidal activity against *Staphylococcus* spp. in the immobilized state and to be compatible to osteoblast-like cells[24,25]. In this study we focused on the mode of action of this membrane-active peptide when immobilized. By applying viability counts, FE-SEM, and a fluorescence microplate assay with a membrane potential-sensitive dye, we tried to understand whether N- and C- oriented analogues, anchored to titanium disks and to a model resin support, were still able to perturb the membrane of *S. epidermidis*. The cytocompatibility to osteoblast-like MG-63 cells was investigated in monoculture and in co-culture with bacteria.

2. Materials and Methods

2.1. Peptide synthesis and characterization

Two pairs of N- and C-cysteinylated (*Cys-(Ahx)$_3$-GRFKRFRKKFKKLFKKLS-NH$_2$* and *GRFKRFRKKFKKLFKKLS-(Ahx)$_3$-Cys*) or N- and C-biotinylated (*Biotin-Lys-(Ahx)$_3$-GRFKRFRKKFKKLFKKLS-NH$_2$* and *GRFKRFRKKFKKLFKKLS-(Ahx)$_3$-Lys-Biotin*) analogues of

the antimicrobial peptide BMAP27(1-18)[24], hereafter referred to as ^{Cys}B27(1-18), B27(1-18)^{Cys}, *Biot*-N-B27(1-18), and B27(1-18)-C-*Biot*, were used in this study (Fig. S1, Supplementary material). B27(1-18)^{Cys} and ^{Cys}B27(1-18) were purchased from NovoPro (Shangai, China). The two biotinylated derivatives were synthesized on a Biotage Initiator+ microwave-assisted automated peptide synthesizer using Fmoc-chemistry, and biotinylated off-line[24]. The quality of purified peptides was confirmed by mass spectrometry with a Q-STAR hybrid quadrupole time-of-flight mass spectrometer (Applied Biosystems/MDS Sciex, Concord, Canada) equipped with an electrospray ion source. Peptide concentration was determined by UV_{257} absorbance[25].

2.2. Titanium sample preparation and physico-chemical characterization

Commercially pure Ti grade II disks of 10mm diameter and 2mm height (Technalloy S.A., Sant Cugat del Vallès, Spain) were polished, extensively washed and activated by oxygen plasma [25]. After reaction with (3-aminopropyl)triethoxysilane (Sigma-Aldrich) and the bifunctional crosslinker N-succinimidyl-3-maleimidopropionate (SMP, Sigma-Aldrich), disks were functionalized with ^{Cys}B27(1-18), or B27(1-18)^{Cys}. The coupling procedure[25] and the designations of titanium samples are reported in Fig. S1A (Supplementary material). The wettability and surface chemical composition of titanium samples were evaluated by Static Contact Angle Measurements (CA) and X-ray photoelectron spectroscopy (XPS) [25].

2.3. Coupling of biotinylated peptides to streptavidin resin beads and determination of resin loading

Biot-N-B27(1-18) and B27(1-18)-C-*Biot* were coupled to streptavidin-resin beads (high performance Sepharose® resin, GE Healthcare Life Sciences) in sterile phosphate buffered solution (PBS) at 4°C overnight [24]. Resin samples (400µL) have been previously extensively washed with PBS by 5min. centrifugation at 300g to remove storage buffer and allowed to react with an equal volume of 1mM solution of each peptide in PBS or biotin as a control. Samples were then allowed

to re-equilibrate at room temperature, centrifuged, and rinsed 5 times with 1.6mL of PBS. The UV_{257} absorbance of resin supernatants was monitored until the absorbance reached the baseline level. Derivatized resins were kept at 4°C. The designations of resin samples are reported in Fig. S1B (Supplementary material).

For resin loading estimation, 400µL aliquots of each resin were washed three times with 1.6mL of sterile water, then peptides were eluted from the resins by addition of 1.6mL 0.05% trifluoroacetic acid. The elution was repeated twice, the obtained supernatants were combined and freeze-dryed. The concentration of the eluted peptides was determined by UV_{257} absorbance.

2.4. Antimicrobial assays

Staphylococcus aureus ATCC 25923 and *Staphylococcus epidermidis* ATCC 35984 were maintained on Mueller-Hinton (MH) agar plates at 4°C. The minimum inhibitory concentration (MIC) of soluble peptides was determined by the standard MIC assay following CLSI guidelines[24]. For titanium-grafted peptides, *S. epidermidis* was cultured overnight and collected by centrifugation, resuspended in sterile PBS for turbidity assessment and finally in MH broth at $1x10^5$CFU/mL. After 2h-incubation at 37°C on titanium disks, previously sterilized by 30min.-treatment with 70% ethanol, adhesion was evaluated by viable count determination. The adherent bacteria were dislodged from titanium surface by vortexing titanium disks in fresh medium according to a previously described procedure[25]. The adhesion experiments were performed in triplicate for each type of surface. Where indicated, parallel samples were processed for electron microscopy.

2.5. Bacterial membrane depolarization/permeabilization assays

Mid-log phase *S. epidermidis* was collected by centrifugation, washed two times with PBS, and resuspended in PBS supplemented with 25mM glucose (PBS-glc) at $1x10^7$ or $1x10^8$CFU/mL as specified. The desired density was assessed by turbidity at 600nm, with reference to previously

determined standards. The suspension at $1x10^8$CFU/mL was incubated in the orbital shaker at 37°C for 15min.. Thereafter, the potential-sensitive dye 3,3'-dipropylthiadicarbocyanine iodide ($diSC_3(5)$) at 0.4µM, and the DNA staining dye propidium iodide (PI) at 5µg/mL final concentrations were added and 200µL of this suspension were dispensed into a black 96-well plate (Optiplate, PerkinElmer). After a short preincubation at 37°C until baseline fluorescence was stabilized, the soluble *Biot*-N-B27(1-18), and B27(1-18)-C-*Biot* were added in duplicate wells at the desired final concentrations. Fluorescence kinetics were then monitored ($diSC_3(5)$, λ_{ex}=652, λ_{em}=672nm; PI, λ_{ex}=535, λ_{em}=617nm) every 0.5min. for 10-20min.. For the resin-anchored peptides, the assay was adapted to a bacterial suspension of $1x10^7$CFU/mL, prepared as described above in PBS-glc. Due to lower bacterial density, measuring of PI fluorescence was not applicable[26]. $diSC_3(5)$ fluorescence kinetics was monitored as above. At the end of incubation (around 30min.), aliquots were withdrawn for viable count determination and for electron microscopy. The killing percentage was calculated with reference to untreated samples.

The release of cytoplasmic material was analyzed on a $3\text{-}6x10^7$CFU/mL bacterial suspension, prepared as above, incubated with free or resin-bound peptides for 1 h at 37°C. Prior to UV absorbance measurement, samples were centrifuged at 300g for 5min. to settle the resin and supernatants centrifuged again at 13200g for 5min. to settle bacteria.

2.6. Field Emission Scanning Electron Microscopy of *S. epidermidis*

The morphology of treated bacteria was investigated by Field Emission Scanning Electron Microscopy (FE-SEM) (JEOL model JSM-7610FPlus). After 2h-incubation at 37°C, titanium disks were extensively rinsed with filtered sterile PBS and fixed with 2.5% (v/v) glutaraldehyde for 30min. at 4°C[25]. Thereafter, thoroughly washed samples were dehydrated in graded series of ethanol solutions (20min. each) and sputter-coated with gold (Sputter Coater K550X, Emitech, Quorum Technologies Ltd, UK). For bacteria in suspension, upon 30min. fluorescence kinetics

samples were collected by centrifugation at 1000×g for 10min. and fixed with 2.5% (v/v) glutaraldehyde in PBS for 1h at 4°C[26]. Fixed bacteria were extensively rinsed with filtered sterile PBS and dehydrated in graded series of ethanol solutions (20 min. each) by centrifuging at each step. Finally, samples were deposited on 0.2µm Isopore polycarbonate membrane filters (MerckMillipore, Burlington, MA, USA) and sputter-coated with a thin gold layer prior to FE-SEM analysis. All images were collected in the secondary electron detection mode. The working distance was set to 8mm, the acceleration voltage to 5keV, and the probe current to 11 to decrease the interaction depth and obtain more detailed information of the bacterial surface. FE-SEM was performed in duplicate for each sample.

2.7. Osteoblast cell culture, osteoblast-bacteria co-culture and confocal microscopy

The human osteoblast-like MG-63 cell line, obtained from ATCC (Manassas, USA), was maintained in Dulbecco's Modified Eagle Medium (DMEM) in a humidified incubator at 37°C and 5% CO_2 atmosphere. DMEM was supplemented with 10% heat inactivated FBS, 2mM L-glutamine, 100units/mL penicillin and 100µg/mL streptomycin. For cytocompatibility evaluation, the viability of the MG-63 cells seeded onto Ti samples was evaluated upon 4h-incubation at 37°C by using the metabolic dye PrestoBlue®, according to manufacturer's instructions. All experiments were performed in triplicate for each type of surface.

The co-culture experiment was performed according to previous studies[25,27,28] with little adaptations. *S. epidermidis* was allowed to adhere to titanium disks for 2h at 37°C. Thereafter the samples were washed with sterile PBS and seeded with freshly resuspended MG-63 cells in antibiotic-free growth medium supplemented with 2% MH broth, at a density of $1x10^4$cells/well. Following 6- and 24h-incubation at 37°C in humidified 5% CO_2, samples were fixed in 3% paraformaldehyde, stained with Alexa Fluor 546-phalloidin and Hoechst 33342 and examined by Confocal Laser Scanning Microscopy (CLSM) with a Leica TCS SP8 microscope equipped with a

405nm diode laser and a tunable white light laser (Leica Microsystems GmbH, Germany). Images were collected as z-stacks in sequential scanning mode using 10x or 100x objectives (NA 0.3 and 1.4, respectively), and are presented as maximum intensity projections. Images were analyzed using ImageJ 1.51w software (NIH, Bethesda, USA) to determine cell area, cell number and surface coverage. All experiments were performed in duplicate for each type of surface.

2.8. Statistical analysis

All data are represented as mean values ± standard deviations. ANOVA with multiple comparisons HSD-Tukey and non-parametric Mann-Whitney U test were used to determine statistically significant differences (IBM SPSS Statistics 20 software, Armonk, USA). Statistical significance was set at p-value < 0.05.

3. Results

3.1. Peptide and study design

Two pairs of N- and C-cysteinylated or biotinylated derivatives of BMAP-27(1-18)[29] were designed (Fig. S1, Supplementary material). Prior to immobilization, the antimicrobial activity of the four peptide analogues in solution was tested in a standard MIC assay against *S. aureus* and *S. epidermidis*. All derivatives showed negligible differences respect to the parental peptide and each pair of the N- and C-modified analogues exhibited the same MIC values (Table S1, Supplementary material).

3.2. Antimicrobial efficacy and cytocompatibility of titanium-immobilized BMAP27(1-18)

The two cysteinylated derivatives were coupled to titanium disks by an established procedure[25]. CA analysis revealed considerable modifications in wettability as a result of each treatment (Fig. S2A, Supplementary material). The XPS spectra (Fig. S2B, Supplementary material) showed an equal increment in carbon (C1s) and nitrogen (N1s), along with reduction of oxygen (O1s) and

titanium (Ti2p) in Ti_A_B27(1-18)^{Cys} and Ti_A_^{Cys}B27(1-18) respect to Ti_A and Ti samples, indicating stable binding of peptide molecules to titanium, without appreciable differences imputable to their orientation.

The biocompatibility of modified titanium surfaces was addressed by seeding Ti samples with the osteosarcoma-derived MG-63 cells, used as a model. The viability of cells attached to Ti_A and peptide-functionalized surfaces, quantified after 4h-incubation by a PrestoBlue® metabolic assay, was comparable to cell viability on bare titanium, which is known for its biocompatibility (Fig. 1A). The antimicrobial efficacy was evaluated against a reference *S. epidermidis* strain as a representative CoNS species with high adhesion ability which was quantified by viability counts of dislodged bacteria following 2h-incubation on titanium samples and washing away of planktonic microorganisms. The CFUs recovered from both peptide-functionalized samples were remarkably lower respect to silanized titanium (Ti_A), and in turn those recovered from Ti_A were lower respect to bare titanium (Ti) (Fig. 1B). Apparently there was no difference between Ti_A_B27(1-18)^{Cys} and Ti_A_^{Cys}B27(1-18).

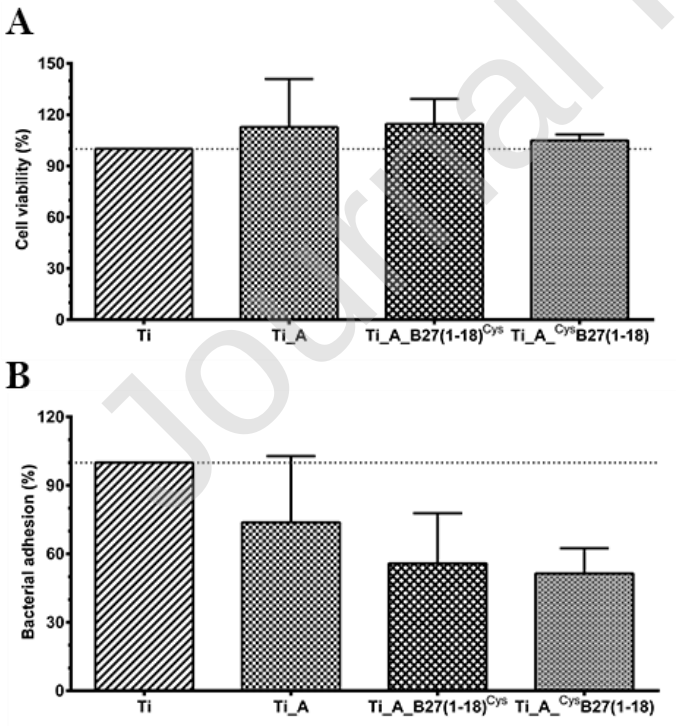

Fig. 1. *(**A**) Cytocompatibility and (**B**) antimicrobial efficacy of peptide-functionalized titanium samples. (**A**) MG-63 osteoblast viability upon adhesion to functionalized Ti samples using the metabolic dye PrestoBlue®. Results are expressed as percent cell viability respect to cells seeded on bare titanium and are the means ± SD of at least three independent experiments performed in triplicate. (**B**) Adhesion of S. epidermidis to the indicated Ti samples. Following 2h-incubation at 37°C, the CFUs of adherent microorganisms were recovered by a vortexing procedure, serial dilutions and plating on solid medium. Results are expressed as percent CFU respect to CFU recovered from bare titanium (Ti) and are the means ± SD of at least three independent experiments performed in triplicate.*

For a deeper investigation of the bactericidal effects mediated by the immobilized peptides, we analyzed the morphology of microorganisms after the 2h-adhesion period by FE–SEM. As evident from representative images in Fig. 2, bacteria displayed remarkable differences in morphology depending on the substrata. *S. epidermidis* cells on Ti and Ti_A controls had normal round shape (Fig. 2A-D), with smooth surface and evident division septa (Fig. 2C-D). Dividing microorganisms often formed multilayer agglomerates (Fig. 2B). In many cases, the typical adhesion structures characteristic of early biofilm, such as tight contact cell-cell junctions and fimbriae-like surface appendages were present (Fig. 2A and C). Furthermore, extracellular matrix elements were also observed (Fig. 2C). *S. epidermidis* cells attached to bare Ti (Fig. 2A) and those attached to silanized Ti disks did not display differences in morphology (Fig. 2B-D).

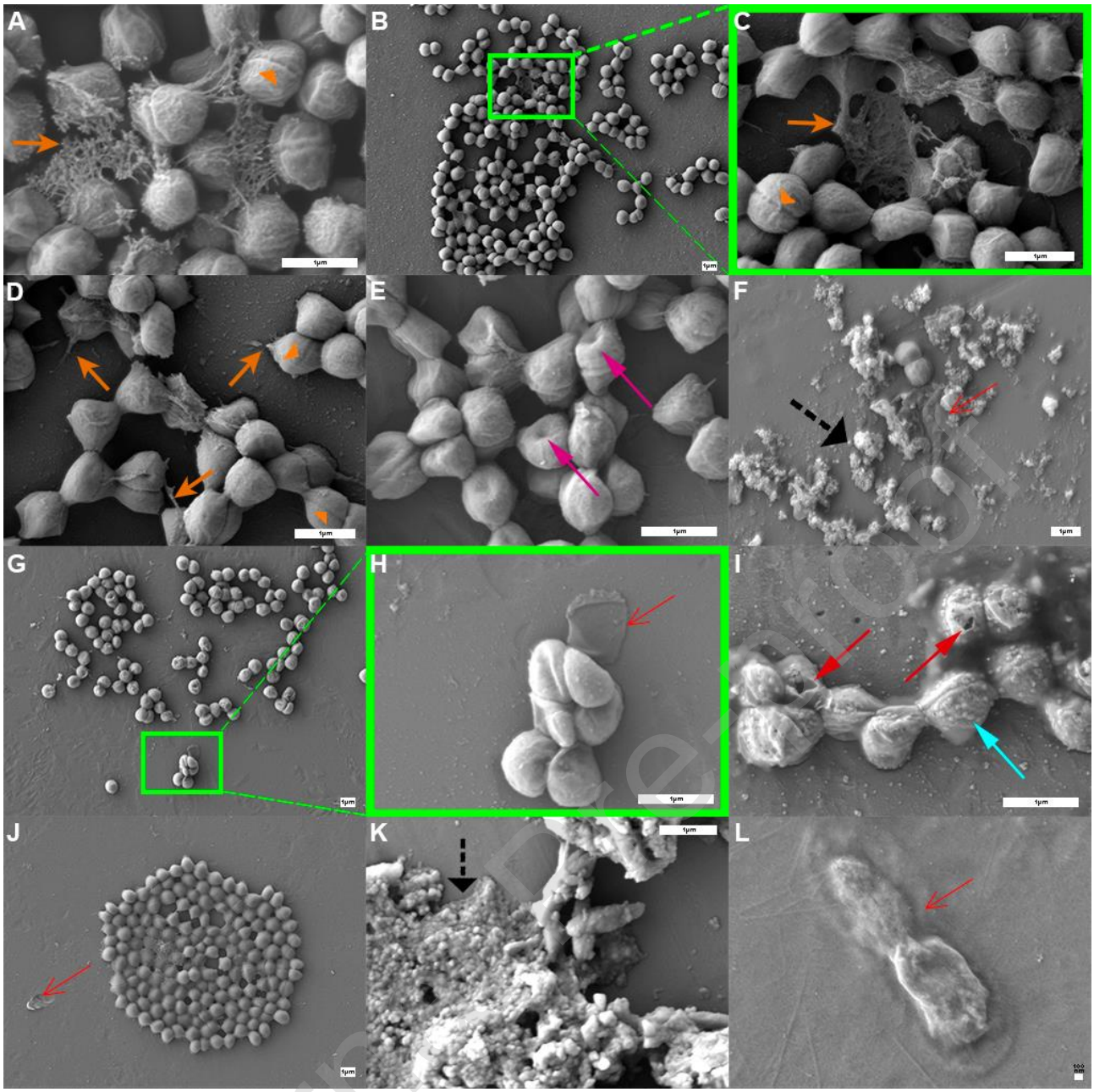

Fig. 2. *Morphology of S. epidermidis on Ti and Ti_A (**Panels A–D**), Ti_A_B27(1-18)^{Cys} (**Panels E–I**) and Ti_A_^{Cys}B27(1-18) (**Panels J–L**) samples analyzed by FE–SEM. Upon 2h-incubation all samples were rinsed, fixed and processed for SEM analysis. **Panels C** and **H** are a higher magnification of the respective images presented in **Panels B** and **G**. Arrows indicate division septa (▶), biofilm structures (↑), amorphous material (⇡), indents (↑), ghosts (⇑), fissures (↑) and blebs(↑). Scale bar denotes 1µm except for L, where denotes 100nm. Representative images from two experiments performed in duplicate are shown.*

Contrariwise, both types of peptide-functionalized titanium samples showed fewer intact *S. epidermidis* cells (Fig. 2E-L). Instead of typical biofilm structures, deflated cells showing indents

(Fig. 2E), remains of dead cells resembling empty bags (Fig. 2H and L), and a lot of amorphous, probably extruded cytoplasmic material from dead cells (Fig. 2F and K), were observed on these samples. Severely damaged cells showing surface blebs (Fig. 2H) and even fissures (Fig. 2I) were observed on Ti_A_B27(1-18)^{Cys} samples, while on Ti_A_^{Cys}B27(1-18) samples it was also possible to note bacterial ghosts, i.e. deflated bacteria with increased size and elongated shape (Fig. 2L).

3.3. Perturbation of *S. epidermidis* cytoplasmic membrane by free and resin-immobilized BMAP27(1-18)

To verify whether N- or C-immobilized BMAP27(1-18) is able to kill bacteria by membrane perturbation, both biotinylated derivatives were coupled to streptavidin-decorated resin beads (Fig. S1B, Supplementary material). Resin loading was estimated in about 250 and 100nmoles/mL of settled resin for the N- and C-immobilized peptide, respectively, as assessed by the determination of the concentration of the resin-eluted peptides. Free and resin-anchored peptides were then compared in a fluorescence microplate assay, which combines the membrane potential-sensitive probe, $diSC_3(5)$, and the membrane impermeable dye, PI[26]. $DiSC_3(5)$ is a cationic carbocyanine with a short alkyl tail[30]. It is membrane-permeable and its accumulation across the polarized membrane in energized cells causes quenching of its fluorescence. Upon membrane depolarization, the dye is quickly released in the medium with fluorescence dequenching[31]. Mid-log phase *S. epidermidis* were first incubated with free biotinylated peptides by kinetically monitoring $diSC_3(5)$ and PI fluorescence. At 30min.-incubation, aliquots were taken for viability counts. The ion channel-forming gramicidin D, used as positive control (100% depolarization)[32], induced increase of $diSC_3(5)$, but not of PI fluorescence (Fig. 3). In contrast, both free peptides at their bactericidal concentrations (1-8µM, i.e. those causing >90% killing), caused a rapid increase of both, $diSC_3(5)$ (Fig. 3A, D) and PI fluorescence (Fig. 3B, E). On the contrary, at lower peptide concentrations

(125-250nM) (Fig. 3C, F), that also produced lower killing, only PI showed an increment, whereas the fluorescence of diSC$_3$(5) remained at baseline level.

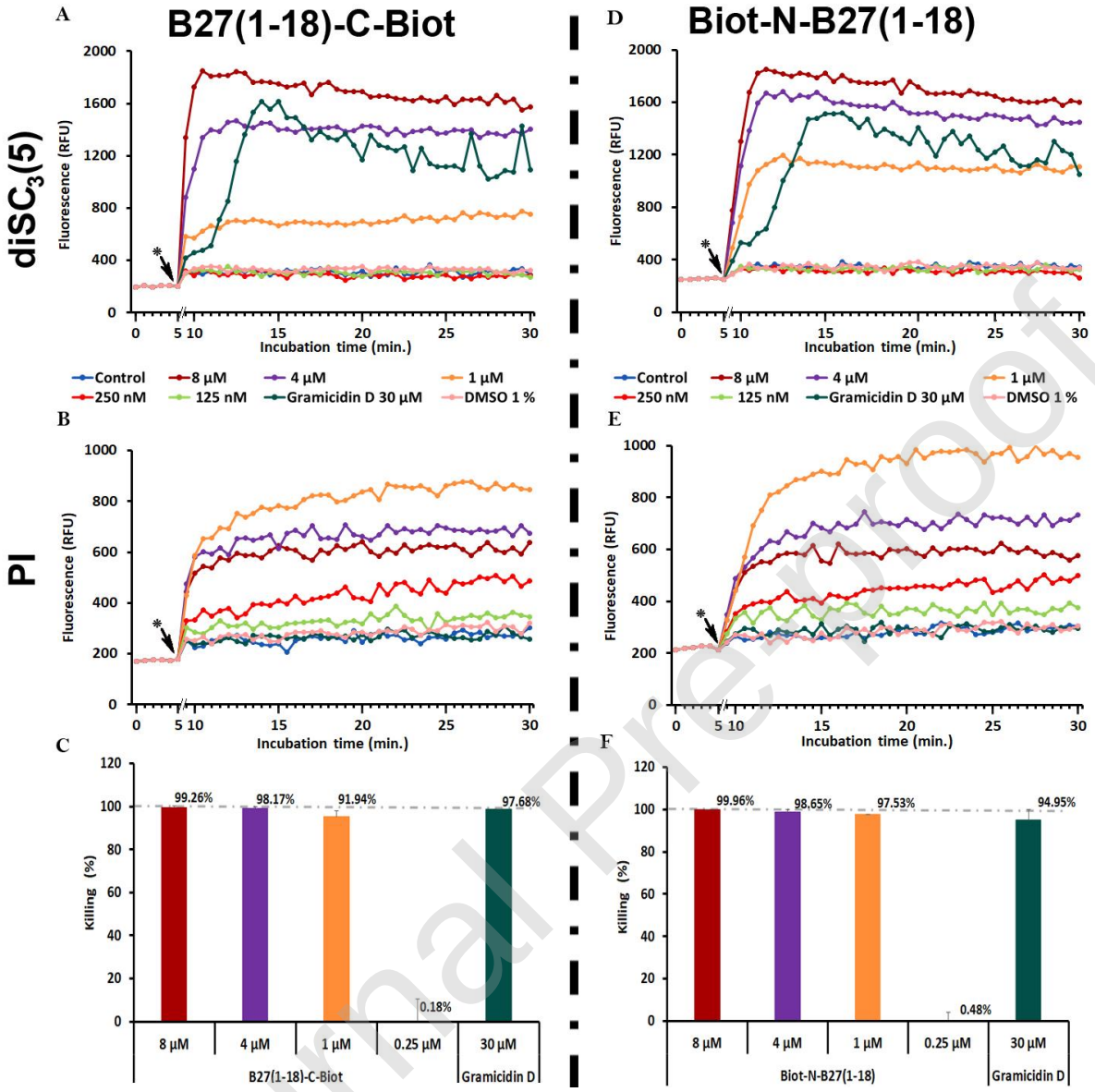

Fig. 3. *Membrane depolarization (**A**, **D**, diSC$_3$(5) fluorescence), permeabilization (**B**, **E**, PI fluorescence) and killing (**C**, **F**, viability counts) of S. epidermidis by soluble B27(1-18)-C-Biot (**A–C**) and Biot-N-B27(1-18) (**D–F**). The experiments were performed with 10^8 CFU/mL in PBS-glc containing 0.4µM diSC$_3$(5) and 5µg/mL PI at 37°C. At 30 min. incubation aliquots were taken to determine bacterial viability by CFU counts. The kinetics of diSC$_3$(5) and PI are shown in separate graphs for clarity purposes. (*) peptide addition.*

Next, the suspension of *S. epidermidis* was incubated with free peptides or their corresponding resin-anchored equivalents in the presence of diSC$_3$(5). Aliquots were withdrawn at 30min.-

incubation to determine bacterial viability. Similar to the previous experiment, both free peptides at 4μM concentration showed the same behavior by promoting a rapid increase of $diSC_3(5)$, correlated to 100% killing (Fig. 4). On the contrary, at an equivalent peptide concentration the resin-bound peptides showed a distinct behavior with the C-terminally immobilized peptide being more active than the N-terminal counterpart. In fact, B27(1-18)-C-resin, at concentrations equivalent to 4 and 8μM free peptide, promoted a dose-related increase of $diSC_3(5)$ fluorescence, correlated to a killing higher than 99% (Fig. 4A and 4C). On the other hand, the same concentration equivalents of the N-terminally bound peptide caused a remarkably lower $diSC_3(5)$ fluorescence, which was nevertheless associated with >90% killing (Fig. 4B-C).

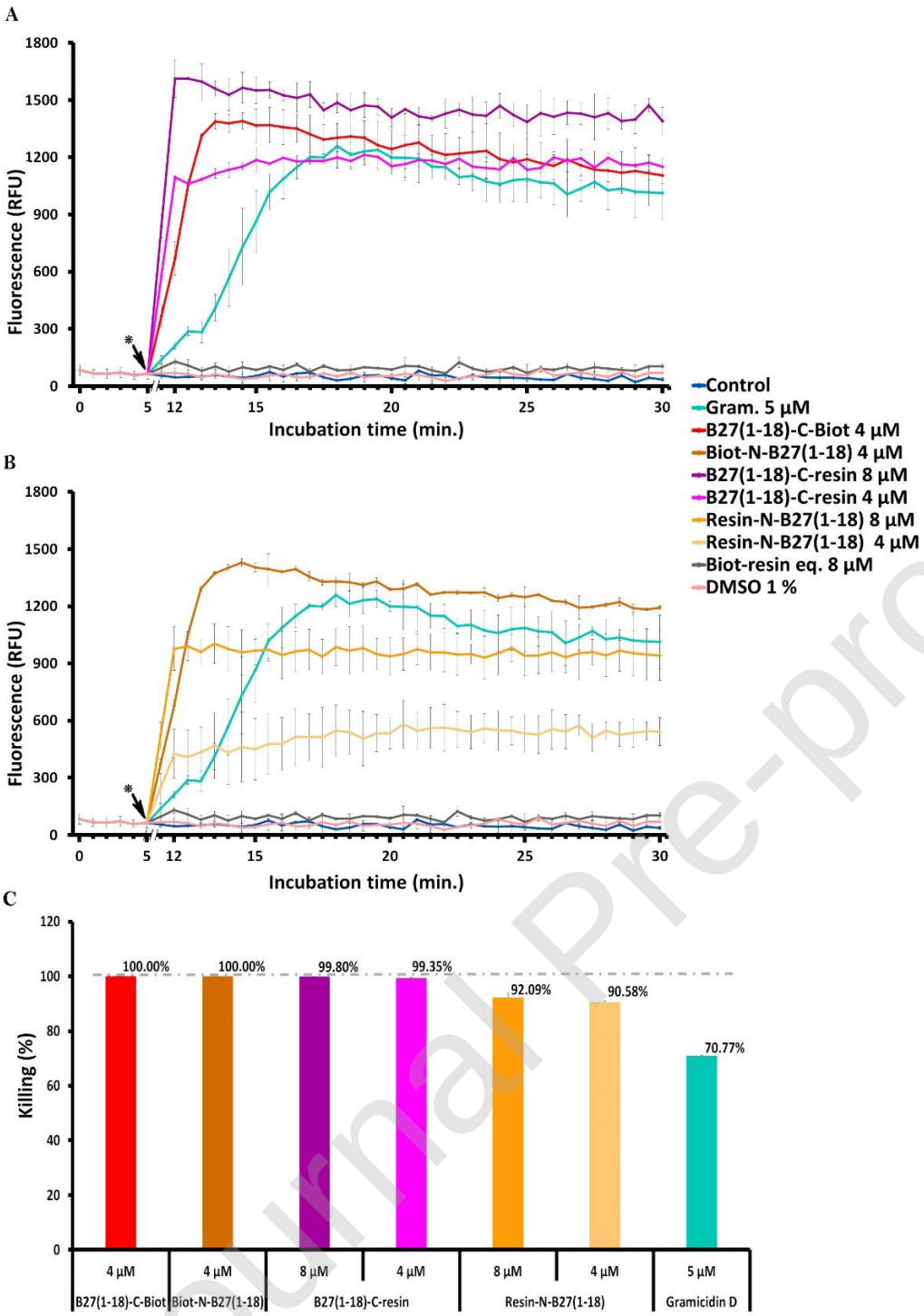

Fig. 4. *Membrane depolarization (**A**, **B**) and Killing (**C**) of S. epidermidis caused by free and resin-bound B27(1-18)-C-Biot and Biot-N-B27(1-18). The experiments were performed with 10^7 CFU/mL in PBS-glc containing 0.4µM diSC_3(5) at 37°C. At 30 min. incubation aliquots were taken to determine bacterial viability by CFU counts. The membrane depolarization caused by each of the*

two peptides is displayed in separate graphs (A and B) for clarity purposes. (*) peptide or resin addition.

To shed light on the events that took place at the staphylococcal surface during mode of action studies, the bacteria morphology upon treatment with free and resin-bound peptides was analyzed by FE-SEM (Fig. 5-6).

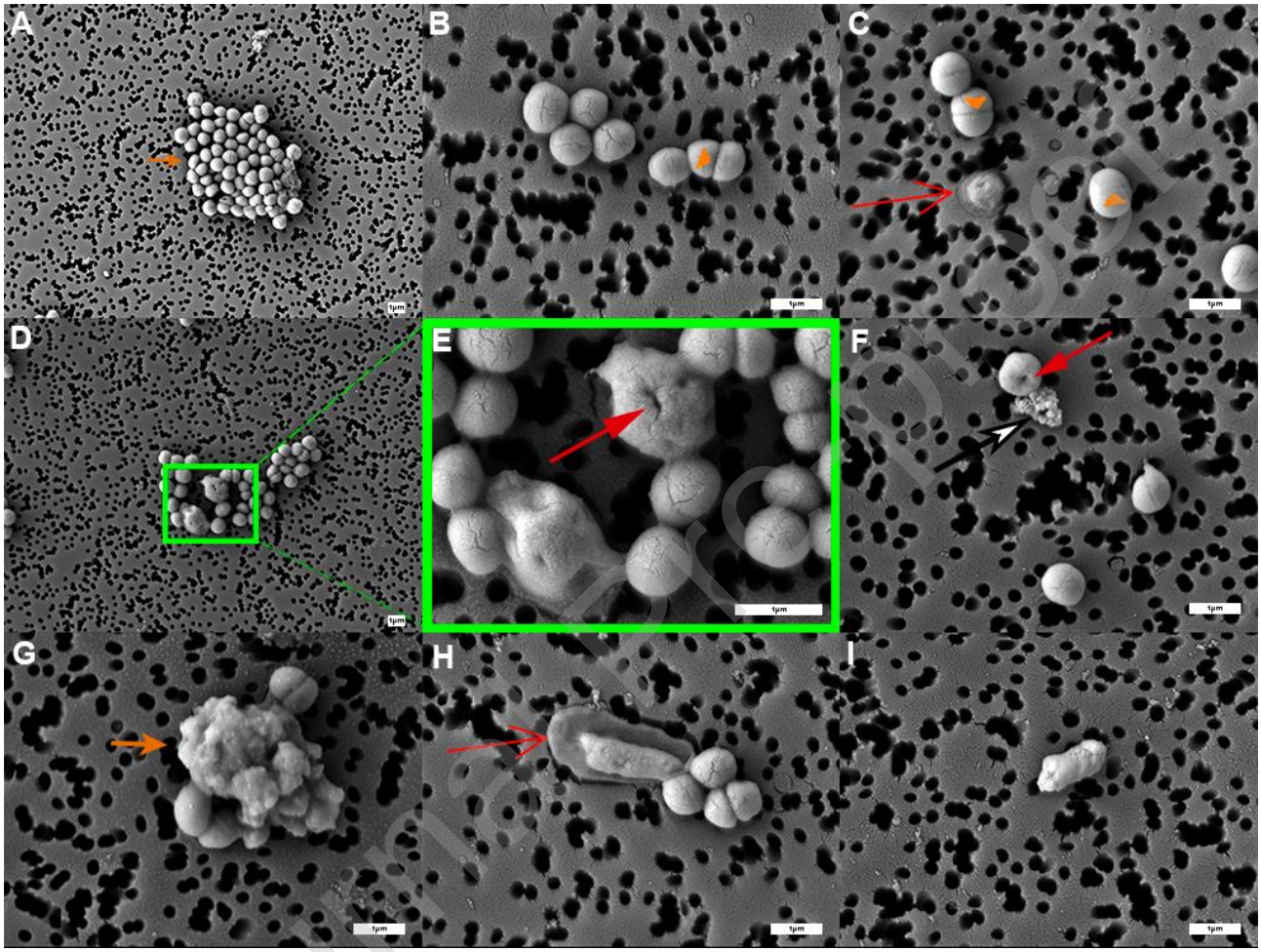

Fig. 5. *Morphology of untreated S. epidermidis (**Panels A–B**), treated with soluble B27(1-18)-C-Biot (**Panels C–G**) or with Biot-N-B27(1-18) (**Panels H–I**), analyzed by FE-SEM. **Panel E** show a higher magnification of the image presented in **Panel D**. Arrows indicate, respectively, division septa (▶), bacterial aggregates (↑), extruded cytoplasmic material (↑), collapsed bacteria (↑), ghosts (↑). Scale bar denotes 1µm. Representative images from two experiments performed in duplicate are shown.*

Biotinylated streptavidin-resin beads were used as negative controls (Fig. 6A-B). Untreated *S. epidermidis* cells and those put in contact with the control resin had normal appearance with clearly evident division septa (Fig. 5A-B and 6A-B). Bacterial cells exhibited the expected size, with an average diameter of 0.8µm, clearly and easily distinguishable from resin beads (roughly 14-18µm, Fig. 6A-B).

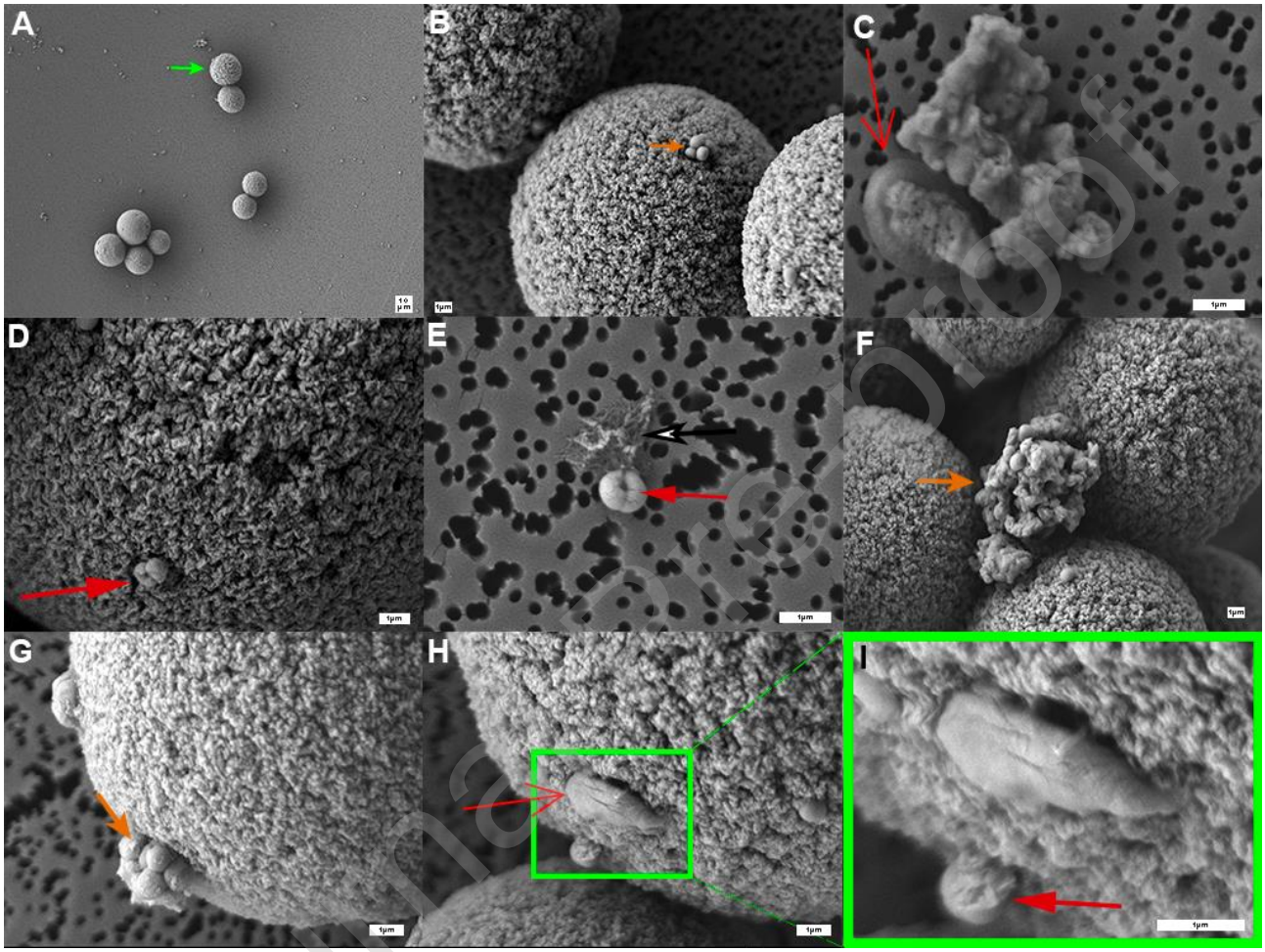

Fig. 6. *Morphology of untreated S. epidermidis (**Panels A–B**), treated with B27(1-18)-C-Biot-Res (**Panels C–F**) or with Res-Biot-N-B27(1-18) (**Panels G–I**), analyzed by FE-SEM. **Panel I** shows a higher magnification of the image presented in **Panel H**. Arrows indicate, respectively, resin beads (↑), bacterial aggregates (↑), extruded cytoplasmic material (↑), collapsed bacteria (↑), ghosts (↑). Scale bar denotes 1µm except for A, where denotes 10µm. Representative images from two experiments performed in duplicate are shown.*

Bacteria formed clusters throughout the filter extension, also on the resin surface (Fig. 5A-7B). Of course, as the assay was performed with bacteria in suspension, typical biofilm structures such as

those visualized in Fig. 2 were not observed. In contrast, the filters containing *S. epidermidis* treated with free biotinylated peptides (4μM) presented a remarkably reduced number of bacteria with some agglomerates (Fig. 5D, G) and many *S. epidermidis* cells were dramatically affected. In some cases, dead bacteria appeared swollen, without division septa (Fig. 5E), in others they were collapsed and somehow melted, appearing to merge into the filter (Fig. 5C, H), or deflated with extrusion of cytoplasmic material out of the cell (Fig. 5F). In several cases, clusters containing a mix of live and dead bacteria (Fig. 5D, G, H) sometimes appearing as a big amorphous mass deposited on filter (Fig. 5G), were observed. A reduced number of *S. epidermidis* cells with some clusters and many morphologically modified bacteria was observed also upon treatment with both resin-bound peptides (4μM resin equivalents) (Fig. 6C-I). In some of the aggregates bacteria showed evident surface blebs (Fig. 6G), while in the others bacteria were entrapped in an amorphous mass (Fig. 6F). Some individual cells attached to resin surface displayed elongated shape without division septa (Fig. 6H-I). In some images bacteria were deflated, or even collapsed, with indents and often with extruded cytoplasmic material (Fig. 6C-E). The release of intracellular content is also supported by the roughly two-fold increased UV-absorbance of sample supernatants upon bacteria incubation with both resin-bound and free peptides at bactericidal concentrations (data not shown).

3.4. Cytocompatibility of titanium-immobilized BMAP27(1-18) in an osteoblast-bacteria co-culture experiment

The functionalized titanium samples were investigated in a co-culture assay to address the "race for the surface" question and to distinguish between a direct microbicidal action and other possible effects on cell adhesion and spreading, related to peptide orientation. Titanium samples were incubated with and without *S. epidermidis* for 2h, then washed, seeded with osteoblast cells and incubated for 6h and 24h. Samples were then fixed and processed for CLSM and images

subsequently analyzed to determine cell numbers (Table S2, Supplementary material), mean cell area values, and cell surface coverage (Fig. 8). Representative images are shown in Fig. 7 and Fig. S3 (Supplementary material).

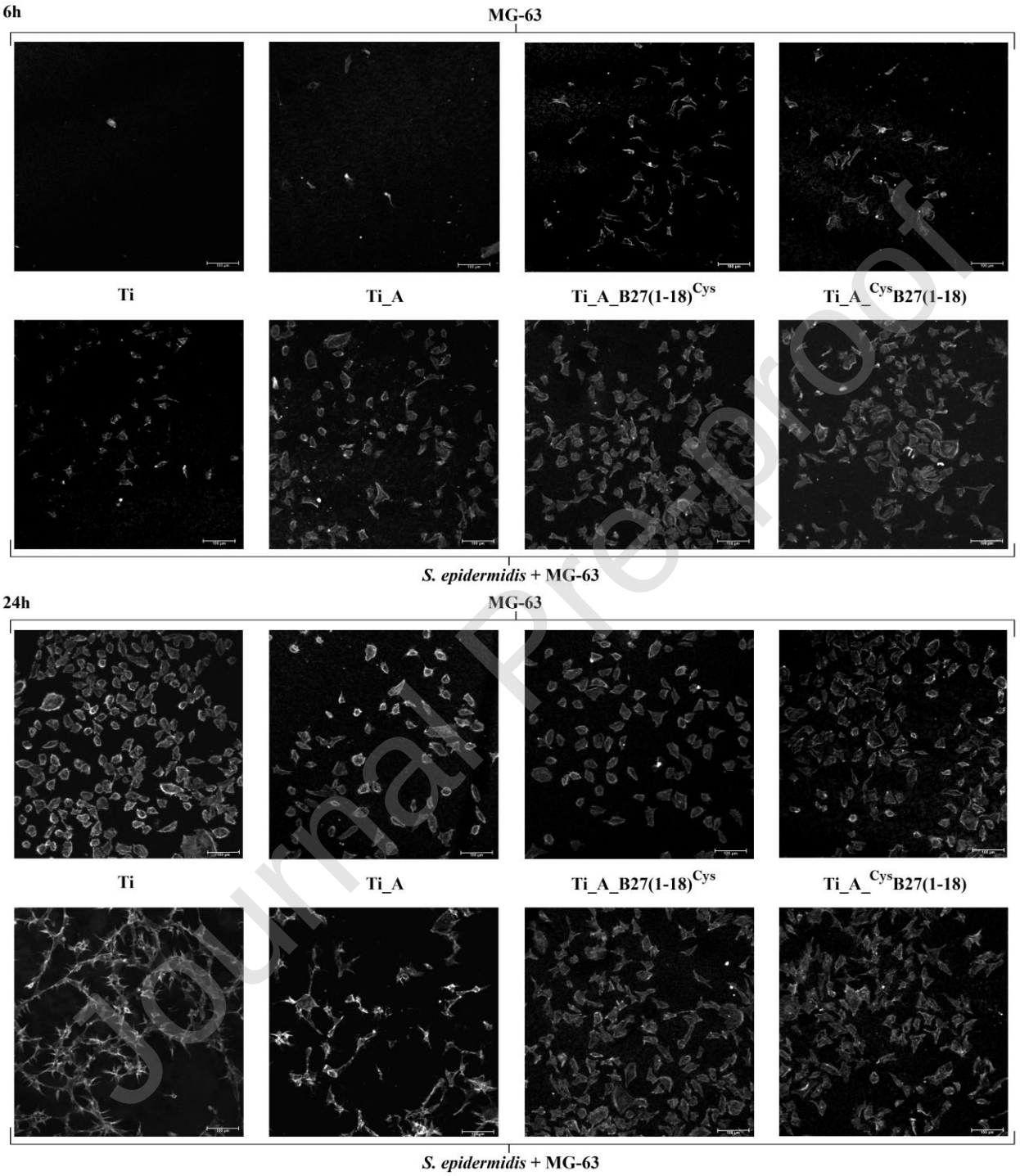

Fig. 7. *Representative confocal images of MG-63 cells adhered to the indicated Ti samples at 6h and 24h in the absence and in the presence of bacteria. At these time points, samples were fixed and*

stained with Alexa Fluor 546-phalloidin and Hoechst. For clarity purposes, only the Alexa-Fluor 546 channel is shown. Scale bar = 100 µm.

At 6h-incubation, mean cell area values were increasingly higher going from Ti to Ti_A to Ti_A_B27(1-18)^{Cys} and Ti_A_^{Cys}B27(1-18), incubated without bacteria (Fig. 8A). A similar increasing trend was also observed for bacteria pre-incubated samples (Fig. 8B). At the same time point the osteoblast numbers on peptide-grafted titanium were around 4-5 times higher than on bare Ti in both conditions (i.e. with or without bacteria) (Fig. 8A-B and Table S2, Supplementary material). Interestingly, at 6h-time point all bacteria pre-incubated samples showed remarkably higher total cell numbers (Fig. 8B and Table S2, Supplementary material).

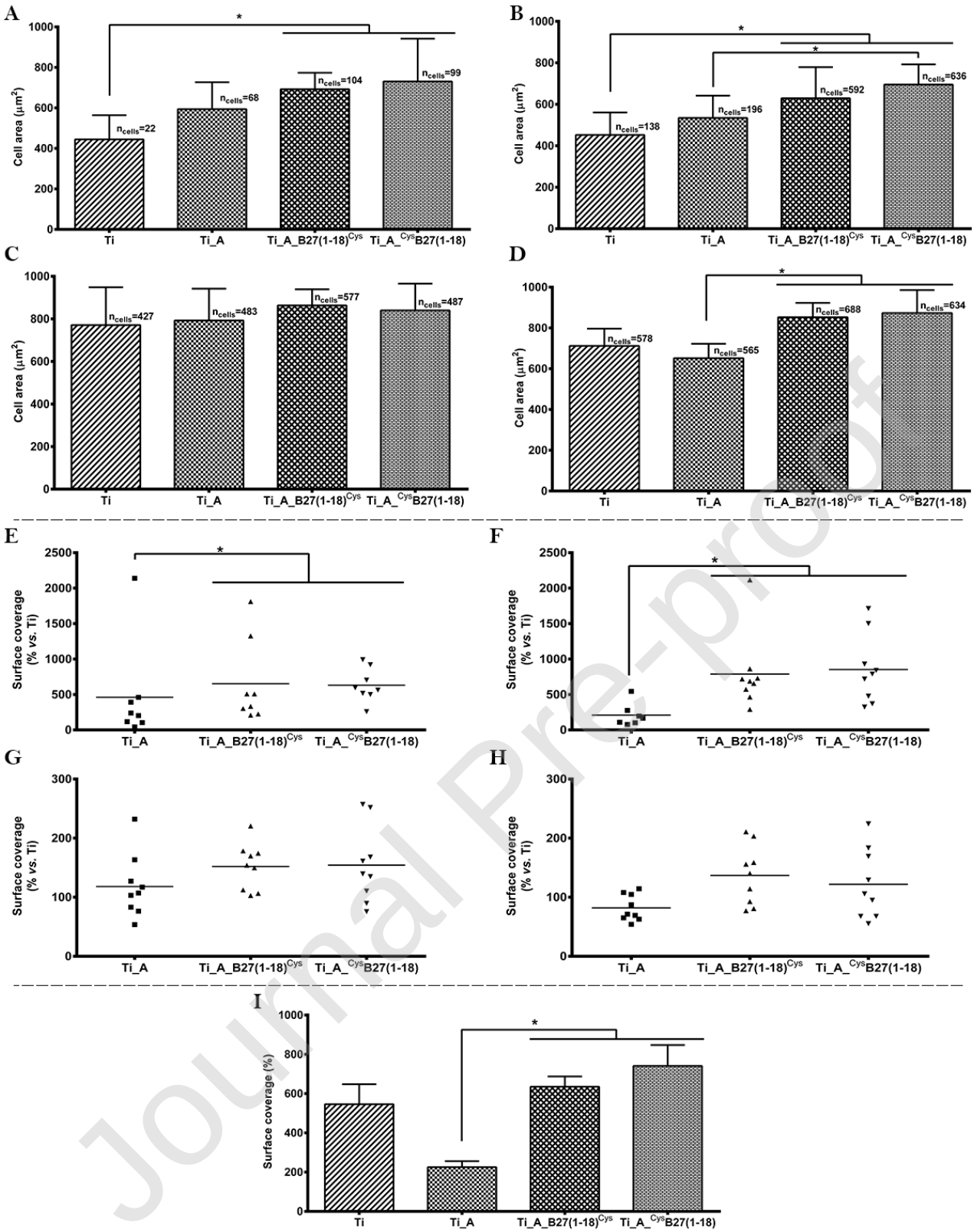

Fig. 8. *MG-63 mean cell area values on the indicated samples at 6h (**A**, **B**) and 24h (**C**, **D**) in the absence (**A**, **C**) and in the presence (**B**, **D**) of bacteria. MG-63 surface coverage percentages on the indicated samples respect to Ti at 6h (**E**, **F**) and 24h (**G**, **H**) in the absence (**E**, **G**) and in the presence (**F**, **H**) of bacteria. **I.** MG-63 surface coverage percentages on the indicated samples in the*

presence of S. epidermidis respect to their respective controls without bacteria at 6h-incubation. Osteoblast cell number (Table S2, see Supplementary material) and morphology were quantified from confocal images based on Alexa Fluor 546-phalloidin signal (Fig. 7). Nine blindly selected fields were analyzed for each condition on duplicate samples. Asterisks denote statistically significant differences between the indicated samples ($P < 0.05$).

At 24h-time point the osteoblast spreading in the absence of bacteria was highly comparable on diverse Ti substrates (Fig. 8C), with cell area values between 750-1000µm^2, and with globally higher cell numbers respect to those detected at 6h (Fig. 8C and Table S2, Supplementary material). On the contrary, upon pre-incubation with bacteria, the mean cell area values on Ti_A_B27(1-18)^{Cys} and Ti_A_^{Cys}B27(1-18), while in line with their corresponding bacteria-free counterparts, were significantly higher respect to Ti_A controls (Fig. 8D). Total cell numbers were increased on all bacteria pre-incubated samples respect to their bacteria-free counterparts at the same time point, but with a higher increase of total cells in Ti and Ti_A than in each peptide-grafted titanium when compared to bacteria-preincubated samples at 6h (Fig. 8A-D and Table S2, Supplementary material). Percent cell surface coverage by taking as 100% the corresponding Ti controls is shown in Fig. 8E-H. At 6h-incubation this analysis revealed significant differences between silanized and peptide-functionalized samples in both conditions (Fig. 8E-F), which were not unexpected given the number of cells observed on these samples (Table S2, Supplementary material). On the contrary, the differences between samples were not significant at 24h, regardless the presence of bacteria (Fig. 8G-H), although the mean values appeared different between silanized and peptide-functionalized samples. For a more proper evaluation of cell-attractive and cell-adhesive properties of peptide-functionalized samples upon bacterial challenge, the osteoblast surface coverage was calculated for each sample type pre-incubated with *S. epidermidis*, taking as 100% the cell surface coverage of the corresponding sample, incubated with cells only. These data, reported in Fig. 8I for the 6h-time point, indicate that osteoblast surface coverage was in general incremented on all samples, with higher values on peptide-functionalized titanium. However, differences between C-

and N-immobilized B27(1-18) derivatives were not observed (Fig. 7-8; Fig. S3 and Table S2, Supplementary material).

4. Discussion

The present study was focused on the mode of action of an immobilized membrane-active AMP. The issue is of relevance for the development of peptide-based infection-resistant biomaterials. The target microorganism was *S. epidermidis*, a Gram-positive skin commensal, which can however cause foreign body related infections due to its ability to adhere to implanted prostheses and form biofilm[2,3]. BMAP27(1-18) is a cationic α-helical peptide with broad spectrum antimicrobial activity in solution without toxic effects towards host cells[24]. It proved bactericidal against *Staphylococcus* species when immobilized on a model support[24] and on titanium[25] *via* its N-terminus. These findings prompted us to investigate its mode of action with the aim of improving the immobilization protocol to achieve better antibacterial performance of the surface immobilized BMAP27(1-18). We asked ourselves whether the immobilized peptide was still able to interact with the bacterial membrane and whether such activity was dependent on peptide orientation. This latter aspect was first addressed by comparing the antimicrobial efficacy of two peptide analogues anchored to titanium *via* the N- or the C-terminus. By applying FE-SEM analysis, we could obtain sharp and detailed images highlighting the biofilm forming ability of *S. epidermidis*. After two hour-adhesion, microorganisms in division phase formed multilayer agglomerates with typical structures of early biofilm (Fig. 2A-D), likely representing extracellular matrix components[33–35], and tightly interconnected individual cells were firmly attached to titanium surface by adhesion structures. Such morphological characteristics are in line with the well-known biofilm properties of *S. epidermidis*, a recognized heavy matrix producer[36,37]. Remarkably, the contact of *S. epidermidis* with peptide-functionalized titanium produced dramatic changes in bacteria morphology (Fig. 2E-L).

Collectively, based on FE-SEM analysis and CFU counts we can reasonably deduce that titanium-immobilized BMAP27(1-18), regardless of its orientation, was able to kill *S. epidermidis*, although FE-SEM images did not provide a clear-cut information on possible different effects between the two analogues. Concerning contact killing, our observations are in line with previous findings[25], while the lack of a significant difference between the N- and the C-terminally oriented peptides appears in contrast with the literature[16,17,21–23,38]. In fact, several studies suggest that the antimicrobial efficacy of tethered peptides could be affected by the position of cationic and hydrophobic residues. In particular, tethering orientation seems important for those AMPs characterized by sequence-dependent amphipathicity with hydrophobic and cationic residues segregated at the N-terminus and the C-terminus, such as melittin[16], melimine[22] or Dhvar[21], while it appears less important for AMPs with conformation-dependent amphipathicity such as temporin-SHa[38]. However, generalizations cannot be made even in the same category, as in some cases peptide orientation affected the activity, but with opposite results[16,21,22]. In the case of the sheep cathelicidin SMAP-29, a peptide highly similar to BMAP-27(1-18)[39], Soares *et al.* registered remarkably better antimicrobial activity with the peptide immobilized *via* its C-terminus[23]. At first glance both peptides seem highly similar with conformation-dependent amphipathicity due to a regular distribution of cationic and hydrophobic residues along the sequence. However, looking in more detail at their N-termini, the first amino acid of SMAP-29 is an Arginine, followed by a Glycine residue, whereas the same amino acids are present at inverted positions (GR instead of RG) [29,39] in BMAP27(1-18). This could at least partly explain why masking of the N-terminal Arg upon tethering of SMAP-29 *via* its N-terminus resulted in decreased activity, whereas killing ability of BMAP27(1-18) seemed not much affected by tethering orientation, as observed in the present as well as in a previous study[24]. An additional indirect evidence that antimicrobial activity of BMAP-27 is relatively independent on anchoring position was provided by Rapsch *et al.*[40]. In that study

the full length BMAP-27 was randomly immobilized on a glass surface by exploiting its amino groups, without any spacer, and the immobilized peptide was active against *E. coli*.

Taken together, these considerations suggest that besides structural features such as amino acid sequence, conformation, and amphipaticity, specific aspects related to peptide mode of action in the immobilized state should also be investigated. In this regard, the capability of immobilized membrane-active peptides to interact and perturb the cytoplasmic membrane of target microorganisms is still poorly characterized. To address this point, we wanted to apply a fluorescence microplate assay which was developed recently with the aim of monitoring peptide-induced changes in membrane polarity and/or permeability on whole bacteria in real time[26]. In order to compare membrane effects of free and anchored BMAP27(1-18), we needed to keep both peptide forms in solution and to know their respective concentrations. We met both requirements by coupling the N- and the C-biotinylated analogues to a commercial resin, functionalized with streptavidin. This approach allowed to mimic an immobilized, yet fluid condition, suitable for the microplate fluorescence assay. Moreover, knowing the peptide loading on the resin, we could make quantitative comparisons between the free and the anchored peptide, and between the two peptide orientations on the resin. The free biotinylated analogues at highly bactericidal concentrations (i.e. 1-8μM) induced increase of both fluorescent dyes, while at suboptimal concentrations (i.e. 125-250nM) only PI fluorescence was increased (Fig. 3). This behavior, remarkably different with respect to that of gramicidin D, was similar to what observed previously with melittin[26], suggesting membrane permeabilization (increase in PI fluorescence) as the primary event in bacteria killing, followed by membrane depolarization (increase in $diSC_3(5)$ fluorescence) as a consequence. Interestingly, at the most effective bactericidal concentrations the increase of PI fluorescence was not dose-dependent (Fig. 3). To explain this lack of proportionality one can argue that when membrane damage is extensive, the highly cationic peptide molecules bind to bacterial DNA[41,42] thus displacing PI, which becomes less fluorescent when unbound. The release of nucleic

acids is also supported by the increase of UV_{260} absorbing material in the supernatants of samples, incubated with free and resin-bound peptides (data not shown).

For resin-anchored peptides, in order to keep the volume of added resin acceptably low and compatible with the fluorescent assay, the density of the bacterial suspension was reduced from $1x10^8$CFU/mL to $1x10^7$CFU/mL, thus precluding the possibility to detect PI fluorescence in combination with that of $diSC_3(5)$[26]. Nevertheless, based on the shape of $diSC_3(5)$ fluorescence kinetics induced by resin-bound peptides, highly similar to those caused by the soluble counterparts (Fig. 4), and to those observed previously with melittin[26], we could reasonably deduce that both peptides in the anchored state acted by permeabilization of the bacterial cell membrane, although with different efficacy. When compared to 4µM (i.e. the MBC) soluble BMAP27(1-18), B27(1-18)-C-resin was almost equally effective in killing *S. epidermidis* (99,35% *vs*. 100%) with a roughly 20% lower increase of $diSC_3(5)$ fluorescence, while the N-terminally immobilized analogue displayed a clearly reduced activity (90% killing with 77% lower increase of $diSC_3(5)$ fluorescence), which was however partly recovered at 8µM peptide-resin equivalents (92% killing with 23% lower increase of $diSC_3(5)$ fluorescence, Fig. 4). This outcome seems in contrast with the bactericidal activity exerted by titanium-grafted BMAP27(1-18), which appeared as orientation-independent (Fig. 1B). However, the two experimental approaches are not directly comparable. Apart from the obvious difference in the nature of the surface and in the immobilization strategy, other experimental parameters such as the density of the bacteria suspension (10^7CFU/mL *vs*. 10^5CFU/mL) and the incubation time may play a role. Concerning incubation time, Li and colleagues reported an interesting correlation, induced by peptide-surface orientation, between structure and activity of the immobilized α-helical peptide MSI-78[43]. In that study the authors demonstrated that MSI-78 adopted a completely different orientation, respect to the glass surface, when grafted on glass through its N- or C-terminus. While in the second case the orientation was "laying down", in the first case it was "standing up", with a faster killing due to a quicker initial

interaction with target bacteria. However, after 60min. incubation both the fast- and the slow-acting MSI-78 orientations reached the same bactericidal effect, meaning that any difference due to orientation was evident at the shorter incubation time only[43]. It is tempting to speculate a similar behavior also for BMAP27(1-18) tethered on different supports, to explain the apparent discrepancy between orientation-dependent and orientation–independent bactericidal activity. Concerning the experiments with titanium samples, any possible difference between BMAP27(1-18) with opposite orientation could become less evident, if not negligible, upon 2h-incubation (Fig. 1B). On the contrary, to understand the difference in activity between the two resin-bound peptides one could speculate that peptide molecules with opposite orientations have distinct ability to interact with target microorganisms, what is evident at short incubation times such as those used in the fluorescence assay (i.e., 0-10min.). Accordingly, the larger difference between B27(1-18)-C-biot-resin and resin-N-biot-B27(1-18) was recorded in $diSC_3(5)$ fluorescence, which was measured in real time, whereas the difference in killing, which requires longer sample processing, was less pronounced (Fig. 4).

FE-SEM images confirmed the ability of resin-immobilized B27(1-18) to kill *S. epidermidis*. Treatment with either free or resin-bound B27(1-18) resulted in strongly reduced bacteria number, with similarly affected morphology, including aggregates of live and dead cells entrapped in an amorphous mass, deflated cells with indents and extruded cytoplasmic material, and collapsed bacteria with completely distorted shape (Fig. 5 and 6). However, the overall picture was highly similar to what observed upon treatment with peptides in solution and lesion peculiarities possibly related to each peptide orientation did not emerge, maybe because the samples for electron microscopy were taken at the end of fluorescence kinetics, i.e. at ~25min. after the addition of peptide-resin equivalents, when presumably the initial interactions with the bacterial membrane were almost completed.

Given the ability of anchored BMAP27(1-18) to perturb the cytoplasmic membrane of *S. epidermidis* leading to a bactericidal effect, it was important to verify whether the integrity of osteoblast cells was also affected. The osteoblast-like MG-63 cells adhered to the titanium surface equally well, regardless of peptide orientation, and expressed good metabolic activity after 4h-incubation on the peptide-functionalized titanium samples (Fig. 1A). Additional interesting findings were obtained by evaluating MG-63 cell adhesion and spreading in the osteoblast-bacteria co-culture experiments, in particular at the 6h-time point. By analyzing mean cell area values on bacteria-preincubated titanium samples, we noticed a higher spreading ability of osteoblast cells on peptide-functionalized titanium disks, respect to bare or silanized titanium (Fig. 8B). This outcome was logically expected given the capability of titanium-grafted peptide to clear away the bacteria, thus favoring better adhesion of MG-63 cells. This finding was consistent with the increased cell numbers, together with increased cell surface coverage, on peptide-functionalized samples, respect to control titanium at the same time point (Fig. 8 and Table S2, Supplementary material). Nevertheless, a similar trend was also observed on parallel samples incubated in the absence of bacteria (Fig. 8A, 8E and Table S2, Supplementary material), suggesting a peptide-mediated effect on osteoblast cell adhesion and spreading, not related to the direct antimicrobial activity of BMAP27(1-18). However, none of our analyses revealed any significant difference between the N- or C-oriented peptide, suggesting an underlying mechanism without need for sequence specificity. Regarding the mode of action of membrane-active peptides on bacteria, this feature is well established[44–46]. Furthermore, many effects elicited by AMPs on host tissue cells are not canonical receptor-mediated phenomena[47]. In this respect it is important to note that antimicrobial peptides free in solution, such as LL-37 and β-defensins, have been reported to promote various processes implicated in bone repair[48–51].

At 24h-time point the differences among samples were less evident, maybe because cells reached a plateau. In monoculture, osteoblast spreading was similar on diverse Ti substrates (Fig. 8C) with

better spreading on peptide-functionalized samples. In general this was true also for cells growing on *S. epidermidis* pre-incubated samples, but in this case, mean cell area values of cells on Ti_A samples were significantly lower respect to Ti_A_B27(1-18)^{Cys} and Ti_A_^{Cys}B27(1-18) (Fig. 8D). In fact, MG-63 cells on contaminated Ti samples were smaller with obvious modifications in morphology as a consequence of biofilm formation, which was clearly evident in some areas of silanized and bare titanium (Fig. S3, Supplementary material) and which was not observed on peptide-functionalized samples. An additional finding of the co-culture experiments was a remarkably higher total cell number in all titanium samples that have been pre-incubated with bacteria, respect to their bacteria-free counterparts (Table S2, Supplementary material). At 6h-incubation the increment was impressive, with 190-540% more cells growing in co-culture respect to monoculture samples, while at 24h the differences were still present, but strongly reduced (16-35% increment). As the ratio of cells in co-culture respect to monoculture has increased proportionately among the samples (Table S2, Supplementary material), one could imagine that the increment observed on peptide-functionalized titanium disks was due to a major availability of nutrients on the titanium surface, as the result of the killing activity exerted by the peptide. However, the increased cell number on bare and silanized titanium could not be related to the presence of BMAP27(1-18). This observation is intriguing because it suggests that bacteria themselves could in some way affect cell adhesion[52]. Taking into account what has been reported for the oral environment[53,54], currently we cannot rule out possible stimulating effects of bacteria on tissue cell expression of adhesion molecules that would in turn improve cell adhesion and spreading. Nevertheless, cell surface coverage data, presented for each condition at each time point respect to bare titanium (Fig.8E-H), or normalized by pairwise comparison of each sample in co-culture respect to monoculture (Fig. 8I), clearly revealed an increase of osteoblast surface coverage on all samples with moderately higher values on BMAP27(1-18) functionalized surface. Hence, the

results of the co-culture experiments indicate that the race for the surface between *S. epidermidis* and the osteoblast-like MG-63 cells was won by the latter.

5. Conclusions

In the present paper, the bactericidal mechanism of a peptide-based biomaterial was elucidated by applying the biotin-streptavidin technology, a microplate fluorescence assay, and electron microscopy. Collectively, data provide clear evidence of membrane perturbation, strongly altered morphology and killing of *S. epidermidis* upon contact with the surface-immobilized BMAP27(1-18), mostly independent on peptide orientation. In addition, the co-culture experiments highlighted the capability of the immobilized peptide to help host tissue cells to win the race for the surface. Taken together, these findings represent a good starting point for the development of infection-resistant biomaterials based on antimicrobial peptides and their derivatives.

CRediT Author statement

Gerard Boix-Lemonche: Conceptualization, Methodology, Validation, Data Curation, Formal Analysis, Investigation, Visualization, Writing – Original Draft, Review & Editing. **Jordi Guillem-Marti:** Conceptualization, Investigation, Validation, Data Curation, Writing – Review & Editing. **Maria Lekka:** Resources, Investigation, Writing – Review & Editing. **Francesca D'Este:** Resources, Investigation, Formal Analysis, Writing – Review & Editing. **Filomena Guida:** Resources, Investigation. **José María Manero:** Supervision, Funding Acquisition, Writing – Review & Editing. **Barbara Skerlavaj:** Supervision, Project Administration, Funding Acquisition, Writing – Review & Editing.

Notes

The authors declare no competing financial interest.

Acknowledgements

The authors acknowledge the financial support of departmental research funds (Department of Medicine, University of Udine, Italy). The authors also gratefully thank the Generalitat de Catalunya for funding through project 2017SGR-1165 and the Ministry of Science and Innovation, Spain, for financial support through the RTI2018-098075-B-C21 project, co-funded by the EU through the European Regional Development Funds.

The authors are grateful to Prof. Alessandro Tossi, Department of Life Sciences, University of Trieste, Italy, for peptide synthesis facility and assistance in mass spectrometry, and to Dr. Alessandra Arzese, Department of Medicine, University of Udine, Italy, for helpful discussion.

The authors are grateful to Prof. Lorenzo Fedrizzi, Polytechnic Department of Engineering and Architecture, University of Udine, Italy, for the use of the Field Emission Scanning Electron Microscope.

Appendix A. Supplementary data

Supplementary data associated with this article can be found, in the online version, at "xxxxx".

REFERENCES

[1] J. Josse, F. Valour, Y. Maali, A. Diot, C. Batailler, T. Ferry, F. Laurent, *Front. Microbiol.* **2019**, *10*, DOI 10.3389/fmicb.2019.01602.

[2] P. Izakovicova, O. Borens, A. Trampuz, *EFORT Open Rev.* **2019**, *4*, 482.

[3] F. Schaumburg, A. S. Alabi, G. Peters, K. Becker, *Clin. Microbiol. Infect.* **2014**, *20*, 589.

[4] K. Becker, C. Heilmann, G. Peters, *Clin. Microbiol. Rev.* **2014**, *27*, 870.

[5] D. Campoccia, L. Montanaro, C. R. Arciola, *Biomaterials* **2013**, *34*, 8533.

[6] H. Chouirfa, H. Bouloussa, V. Migonney, C. Falentin-Daudré, *Acta Biomater.* **2019**, *83*, 37.

[7] F. Costa, I. F. Carvalho, R. C. Montelaro, P. Gomes, M. C. L. Martins, *Acta Biomater.* **2011**, *7*, 1431.

[8] R. E. W. Hancock, H.-G. Sahl, *Nat. Biotechnol.* **2006**, *24*, 1551.

[9] G. Wang, B. Mishra, K. Lau, T. Lushnikova, R. Golla, X. Wang, *Pharmaceuticals* **2015**, *8*, 123.

[10] A. T. Y. Yeung, S. L. Gellatly, R. E. W. Hancock, *Cell. Mol. Life Sci.* **2011**, *68*, 2161.

[11] L. T. Nguyen, E. F. Haney, H. J. Vogel, *Trends Biotechnol.* **2011**, *29*, 464.

[12] T. Koprivnjak, A. Peschel, *Cell. Mol. Life Sci.* **2011**, *68*, 2243.

[13] A. Andrea, N. Molchanova, H. Jenssen, *Biomolecules* **2018**, *8*, 27.

[14] M. Riool, A. de Breij, J. W. Drijfhout, P. H. Nibbering, S. A. J. Zaat, *Front. Chem.* **2017**, *5*, 1.

[15] M. Bagheri, M. Beyermann, M. Dathe, *Antimicrob. Agents Chemother.* **2009**, *53*, 1132.

[16] M. Bagheri, M. Beyermann, M. Dathe, *Bioconjug. Chem.* **2012**, *23*, 66.

[17] K. Hilpert, M. Elliott, H. Jenssen, J. Kindrachuk, C. D. Fjell, J. Körner, D. F. H. Winkler, L. L. Weaver, P. Henklein, A. S. Ulrich, et al., *Chem. Biol.* **2009**, *16*, 58.

[18] M. Yasir, D. Dutta, N. Kumar, M. D. P. Willcox, *Biofouling* **2020**, *36*, 1.

[19] M. Gabriel, K. Nazmi, E. C. Veerman, A. V. Nieuw Amerongen, A. Zentner, *Bioconjug. Chem.* **2006**, *17*, 548.

[20] S. A. Onaizi, S. S. J. Leong, *Biotechnol. Adv.* **2011**, *29*, 67.

[21] F. M. T. A. Costa, S. R. Maia, P. A. C. Gomes, M. C. L. Martins, *Biomaterials* **2015**, *52*, 531.

[22] R. Chen, M. D. P. Willcox, N. Cole, K. K. K. Ho, R. Rasul, J. A. Denman, N. Kumar, *Acta Biomater.* **2012**, *8*, 4371.

[23] J. W. Soares, R. Kirby, L. A. Doherty, A. Meehan, S. Arcidiacono, *J. Pept. Sci.* **2015**, *21*, 669.

[24] F. D'Este, D. Oro, G. Boix-Lemonche, A. Tossi, B. Skerlavaj, *J. Pept. Sci.* **2017**, *23*, 777.

[25] G. Boix-Lemonche, J. Guillem-Marti, F. D'Este, J. M. Manero, B. Skerlavaj, *Colloids Surfaces B Biointerfaces* **2020**, *185*, 110586.

[26] G. Boix-Lemonche, M. Lekka, B. Skerlavaj, *Antibiotics* **2020**, *9*, 92.

[27] M. Godoy-Gallardo, J. Guillem-Marti, P. Sevilla, J. M. Manero, F. J. Gil, D. Rodriguez, *Mater. Sci. Eng. C* **2016**, *59*, 524.

[28] B. Zhao, H. C. Van Der Mei, G. Subbiahdoss, J. De Vries, M. Rustema-Abbing, R. Kuijer, H. J. Busscher, Y. Ren, *Dent. Mater.* **2014**, *30*, 716.

[29] B. Skerlavaj, R. Gennaro, L. Bagella, L. Merluzzi, A. Risso, M. Zanetti, *J. Biol. Chem.* **1996**, *271*, 28375.

[30] E. J. A. Veldhuizen, V. A. F. Schneider, H. Agustiandari, A. van Dijk, J. L. M. Tjeerdsma-van Bokhoven, F. J. Bikker, H. P. Haagsman, *PLoS One* **2014**, *9*, 1.

[31] A. Waggoner, *J. Membr. Biol.* **1976**, *27*, 317.

[32] D. A. Kelkar, A. Chattopadhyay, *Biochim. Biophys. Acta - Biomembr.* **2007**, *1768*, 2011.

[33] D. L. Williams, R. D. Bloebaum, *Microsc. Microanal.* **2010**, *16*, 143.

[34] B. Valdez-Salas, E. Beltrán-Partida, S. Castillo-Uribe, M. Curiel-Álvarez, R. Zlatev, M. Stoytcheva, G. Montero-Alpírez, L. Vargas-Osuna, *Molecules* **2017**, *22*, 832.

[35] P. Cao, Y. Yang, F. Uche, S. Hart, W.-W. Li, C. Yuan, *Int. J. Mol. Sci.* **2018**, *19*, 793.

[36] M. Sabaté Brescó, L. G. Harris, K. Thompson, B. Stanic, M. Morgenstern, L. O'Mahony, R. G. Richards, T. F. Moriarty, *Front. Microbiol.* **2017**, *8*, DOI 10.3389/fmicb.2017.01401.

[37] P. D. Fey, M. E. Olson, *Future Microbiol.* **2010**, *5*, 917.

[38] N. Masurier, J.-B. Tissot, D. Boukhriss, S. Jebors, C. Pinese, P. Verdié, M. Amblard, A. Mehdi, J. Martinez, V. Humblot, et al., *J. Mater. Chem. B* **2018**, *6*, 1782.

[39] B. Skerlavaj, M. Benincasa, A. Risso, M. Zanetti, R. Gennaro, *FEBS Lett.* **1999**, *463*, 58.

[40] K. Rapsch, F. F. Bier, M. Tadros, M. von Nickisch-Rosenegk, *Bioconjug. Chem.* **2014**, *25*, 308.

[41] S. Sandgren, A. Wittrup, F. Cheng, M. Jönsson, E. Eklund, S. Busch, M. Belting, *J. Biol. Chem.* **2004**, *279*, 17951.

[42] C.-H. Hsu, C. Chen, M.-L. Jou, A. Y.-L. Lee, Y.-C. Lin, Y.-P. Yu, W.-T. Huang, S.-H. Wu, *Nucleic Acids Res.* **2005**, *33*, 4053.

[43] Y. Li, S. Wei, J. Wu, J. Jasensky, C. Xi, H. Li, Y. Xu, Q. Wang, E. N. G. Marsh, C. L. Brooks, et al., *J. Phys. Chem. C* **2015**, *119*, 7146.

[44] A. Di Grazia, F. Cappiello, H. Cohen, B. Casciaro, V. Luca, A. Pini, Y. P. Di, Y. Shai, M. L. Mangoni, *Amino Acids* **2015**, *47*, 2505.

[45] J. Kindrachuk, E. Scruten, S. Attah-Poku, K. Bell, A. Potter, L. A. Babiuk, P. J. Griebel, S. Napper, *Biopolymers* **2011**, *96*, 14.

[46] M. Mardirossian, A. Pompilio, M. Degasperi, G. Runti, S. Pacor, G. Di Bonaventura, M. Scocchi, *Front. Chem.* **2017**, *5*, 1.

[47] D. Xhindoli, S. Pacor, M. Benincasa, M. Scocchi, R. Gennaro, A. Tossi, *Biochim. Biophys. Acta - Biomembr.* **2016**, *1858*, 546.

[48] M. Kittaka, H. Shiba, M. Kajiya, T. Fujita, T. Iwata, K. Rathvisal, K. Ouhara, K. Takeda, T. Fujita, H. Komatsuzawa, et al., *Peptides* **2013**, *46*, 136.

[49] Z. Zhang, J. E. Shively, *PLoS One* **2010**, *5*, e13985.

[50] Z. Zhang, J. E. Shively, *PLoS One* **2013**, *8*, e67649.

[51] D. Kraus, J. Deschner, A. Jäger, M. Wenghoefer, S. Bayer, S. Jepsen, J. P. Allam, N. Novak, R. Meyer, J. Winter, *J. Cell. Physiol.* **2012**, *227*, 994.

[52] S. N. Somayaji, Y. M. Huet, H. E. Gruber, M. C. Hudson, *J. Biomed. Mater. Res. Part A* **2010**, *95A*, 574.

[53] M. Engels-Deutsch, S. Rizk, Y. Haïkel, *Arch. Oral Biol.* **2011**, *56*, 22.

[54] P. R. Kramer, A. JanikKeith, Z. Cai, S. Ma, I. Watanabe, *Dent. Mater.* **2009**, *25*, 877.